The Madden–Julian Oscillation's Impacts on Worldwide Tropical Cyclone Activity

PHILIP J. KLOTZBACH

Department of Atmospheric Science, Colorado State University, Fort Collins, Colorado

(Manuscript received 14 August 2013, in final form 20 November 2013)

ABSTRACT

The 30–60-day Madden–Julian oscillation (MJO) has been documented in previous research to impact tropical cyclone (TC) activity for various tropical cyclone basins around the globe. The MJO modulates large-scale convective activity throughout the tropics, and concomitantly modulates other fields known to impact tropical cyclone activity such as vertical wind shear, midlevel moisture, vertical motion, and sea level pressure. The Atlantic basin typically shows the smallest modulations in most large-scale fields of any tropical cyclone basins; however, it still experiences significant modulations in tropical cyclone activity. The convectively enhanced phases of the MJO and the phases immediately following them are typically associated with above-average tropical cyclone frequency for each of the global TC basins, while the convectively suppressed phases of the MJO are typically associated with below-average tropical cyclone frequency. The number of rapid intensification periods are also shown to increase when the convectively enhanced phase of the MJO is impacting a particular tropical cyclone basin.

1. Introduction

The Madden–Julian oscillation (MJO) (Madden and Julian 1972) is a large-scale mode of tropical variability that propagates around the globe on an approximately 30–60-day time scale. As it does so, it alters large-scale fields known to impact tropical cyclone (TC) activity, such as vertical wind shear, vertical motion, relative vorticity, and low- and midlevel moisture. Gray (1979) was one of the first to note that TCs tend to cluster in time, with active periods of one to two weeks followed by quieter periods of similar length. More recently, Camargo et al. (2009) examined global TCs and showed that they were significantly modulated by the MJO.

The MJO has been shown to modulate TC activity in each of the global TC basins individually. In the North Atlantic basin, Maloney and Hartmann (2000b) demonstrated that Gulf of Mexico TC activity was much more frequent when lower-tropospheric wind anomalies associated with the MJO were westerly in the eastern Pacific than when they were easterly. Barrett and Leslie (2009) showed that enhanced upper-tropospheric divergence associated with the MJO was one of the primary drivers of increased TC activity in the Atlantic. Klotzbach (2010) and Ventrice et al. (2011) focused on the MJO's impacts on Atlantic basin main development region (MDR) TCs, showing that, when convection was enhanced in the Indian Ocean, TC activity in the Atlantic MDR was increased. Klotzbach (2012) showed that rapid intensification (RI) likelihood also increased when MJO-associated convection was enhanced in the Indian Ocean.

In the northeast Pacific basin, Maloney and Hartmann (2000a) showed that TC development increased when MJO-associated low-level westerly wind anomalies were present in the basin. Aiyyer and Molinari (2008) described an amplified MJO event in August–September 1998 and showed that TC formations were enhanced in the northeast Pacific as the convectively enhanced phase of the MJO passed over the basin. Barrett and Leslie (2009) documented increased TC formation in the northeast Pacific when upper-level divergence was located near 120°W. Klotzbach and Blake (2013) focused on the north-central Pacific (west of 120°W) and showed that convective enhancement associated with the MJO over the eastern and central Pacific led to an increased likelihood for north-central Pacific TC development.

Liebmann et al. (1994) documented a significant increase in northwest Pacific TCs associated with the convectively active phase of the MJO. They attributed this increase to enhanced low-level cyclonic vorticity, and upper-level divergence anomalies typically experienced

Corresponding author address: Philip J. Klotzbach, Department of Atmospheric Science, Colorado State University, 3915 W. Laporte Ave., Fort Collins, CO 80523.
E-mail: philk@atmos.colostate.edu

DOI: 10.1175/JCLI-D-13-00483.1

poleward and westward of the maximum convective enhancement. Kim et al. (2008) and Li and Zhou (2013) have also documented a basinwide increase in northwest Pacific TCs associated with the convectively enhanced phase of the MJO over the region, while noting that the convectively suppressed phase of the MJO typically resulted in reduced TC activity.

Liebmann et al. (1994) found a similar increase in north Indian TCs when the convectively enhanced phase of the MJO was propagating through the region. More recently, Kikuchi and Wang (2010) found that north Indian TC development was favored when convection was enhanced over the Malay Peninsula and dry conditions were present over most of the Indian Ocean. Krishnamohan et al. (2012) showed that Bay of Bengal TCs were enhanced when the MJO's convectively enhanced phase was over the Maritime Continent and eastern parts of the Indian Ocean.

The convectively enhanced phase of the MJO was also shown to enhance TC formation in the south Indian Ocean according to early work by Liebmann et al. (1994). Bessafi and Wheeler (2006) confirmed this result and attributed the increases in TC activity to favorable anomalies in the low-level vorticity and vertical shear patterns. Ho et al. (2006) also found frequent TC occurrences when convection was enhanced in the Indian Ocean and noted that the area of enhanced TC formation in the south Indian Ocean moved eastward with the eastward propagation of the MJO. Recently, Leroy and Wheeler (2008) have utilized this information to make intraseasonal statistical forecasts for all Southern Hemisphere TCs, including the south Indian and South Pacific regions.

Hall et al. (2001) showed that significantly more TCs formed in the Australian region when the convectively enhanced phase of the MJO was present. They attributed this increase to large-scale atmospheric factors, with an emphasis on low-level vorticity.

The impact of the MJO on South Pacific TCs has also been shown. Chand and Walsh (2010) documented dramatic differences in TC genesis near Fiji, with approximately five times more TCs forming in the active phase of the MJO compared with the inactive phase.

Recently, Ramsay et al. (2012) has conducted a cluster analysis of TCs in the Southern Hemisphere and has found that the MJO enhances south Indian TC genesis when the MJO favors convective enhancement in the same region. South Pacific TC activity is favored when the MJO-enhanced convection is located over the western Pacific and Western Hemisphere.

This paper aims to expand upon the previous research by summarizing the results using a consistent metric for the MJO and a state-of-the-art reanalysis product for analysis of large-scale environmental conditions. In addition, this will be the first time to the author's knowledge that any documentation of the relationship between global rates of rapid intensification and the MJO have been conducted. Section 2 discusses the data and methodologies utilized in this manuscript, while section 3 examines how large-scale conditions, TC activity, and rapid intensification frequency are modulated by the MJO in the North Atlantic. Section 4 evaluates MJO-driven fluctuations in the northeast Pacific, while section 5 evaluates MJO-driven fluctuations in the northwest Pacific. Similar examinations for the north Indian, south Indian, and South Pacific are conducted in sections 6 through 8, respectively. Section 9 summarizes the manuscript and provides some ideas for future work.

2. Data and methodology

The daily phase of the MJO was determined from the methodology outlined in Wheeler and Hendon (2004) (hereafter the WH index; available online at http://cawcr.gov.au/staff/mwheeler/maproom/RMM/RMM1RMM2.74toRealtime.txt). They utilized a multivariate EOF analysis to isolate the signal of the MJO by examining signals in both upper- and lower-level zonal winds along with outgoing longwave radiation (OLR). The two principal component (PC) time series that make up the WH MJO index are referred to as the Real-Time Multivariate MJO series 1 and 2 (RMM1 and RMM2). Their index is constructed by first removing the 120-day mean along with interannual variability associated with large-scale phenomena such as ENSO. This index is available from 1974 to present, with data missing for most of 1978 owing to issues with observations of OLR. In this analysis, only days when the WH index is greater than or equal to one are considered. Other equatorial waves, such as Kelvin waves and equatorial Rossby waves, have been shown to imprint themselves on the WH index (Roundy et al. 2009); however, given the long period of this analysis, the MJO is likely the primary signal being detected.

The WH index is classified into eight phases, where the current phase of the MJO is related to where the MJO is having its maximum enhancing effect on deep convection. The maximum OLR anomalies tend to be skewed toward the summer hemisphere, with this effect being more significant during the Northern Hemisphere summer (Madden and Julian 1994). Phases 2 and 3 are associated with convective enhancement over the Indian Ocean, phases 4 and 5 are associated with convective enhancement over the Maritime Continent, phases 6 and 7 are associated with convective enhancement over the Pacific Ocean, and phases 8 and 1 are associated with convective enhancement over the Western Hemisphere.

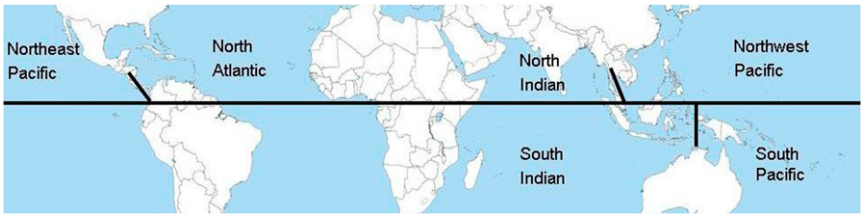

FIG. 1. Global tropical cyclone basin boundaries, as defined for this study.

The large-scale field calculations were calculated from the European Centre for Medium-Range Weather Forecasts (ECMWF) Interim Re-Analysis (ERA-Interim) (Dee et al. 2011) except for OLR. The ERA-Interim reanalysis was downloaded on a 0.75° by 0.75° grid from the ECMWF website (http://apps.ecmwf.int/datasets/data/interim_full_daily/). OLR was calculated from the National Oceanic and Atmospheric Administration (NOAA) interpolated OLR dataset, which is available on a 2.5° by 2.5° grid (Liebmann and Smith 1996).

TC statistics for the Atlantic and northeast Pacific basins were calculated from the Atlantic and northeast Pacific hurricane databases (HURDAT) maintained by the National Hurricane Center (NHC) (Jarvinen et al. 1984; Davis et al. 1984). Joint Typhoon Warning Center (JTWC) data were utilized for the remainder of the global TC basins (e.g., northwest Pacific, north Indian, south Indian, and South Pacific Oceans) (Chu et al. 2002). The JTWC dataset was utilized rather than the World Meteorological Organization warning centers for the remainder of the globe due to the consistency of wind-averaging times (e.g., maximum 1-min sustained winds) for all basins. All TC datasets were downloaded from Unisys Weather (http://weather.unisys.com/hurricane/index.php). Both HURDAT and JTWC datasets provide 6-hourly information on storm location and intensity. TC indices calculated for all basins are as follows: named storms (NS), hurricanes (H), major hurricanes (MH), and accumulated cyclone energy (ACE). Both the HURDAT database and the JTWC database utilize 1-min sustained winds, and the definitions of NS, H, and MH are as follows: NS are TCs with sustained winds of 34 kt (1 kt $\approx 0.51\ \mathrm{m\,s^{-1}}$) or greater, H are TCs with sustained winds of 64 kt or greater, and MH are TCs with sustained winds of 96 kt or greater. ACE is calculated by summing the squares of the maximum 1-min sustained wind for each 6-hourly interval when a TC is at least at NS strength (Bell et al. 2000). TCs that formed in a particular phase of the MJO are assigned to a respective MJO phase based upon day of NS formation. For example, if a TC forms in MJO phase 1 and reaches MH status in a different MJO phase, it would be classified as a MH for MJO phase 1. This is done regardless of the MJO phase on the day that the storm reached the more intense threshold, in keeping with the approach outlined in Klotzbach (2010).

Statistics for RI are calculated only for TCs that had an initial wind speed at or above tropical-storm strength. This methodology helps to prevent issues with tropical depression classifications. RI is calculated over a 24-h period, with a threshold for RI of 30 kt examined in this manuscript, similar to the definition used in Kaplan and DeMaria (2003). There are likely increased uncertainties with both RI and ACE values prior to the mid-1980s when the Dvorak enhanced IR technique (Dvorak 1982) was generally adopted by both NHC and JTWC; however, these uncertainties are likely to be spread across all MJO phases and, therefore, are not expected to impact the results demonstrated here significantly.

Figure 1 displays the geographical boundaries for each TC basin. Statistics for a particular TC are calculated based upon the basin in which the storm formed. Central America is used as the dividing line between the Atlantic and northeast Pacific basins. The international date line is used as the boundary between the northeast Pacific and northwest Pacific basins. The Indonesian subcontinent was utilized as the boundary between the northwest Pacific and north Indian Oceans. The South Pacific and south Indian Ocean basins were split at 135°E, with TCs forming west of this line classified as south Indian TCs and east of this line classified as South Pacific TCs.

To distinguish significance in TC activity for a particular phase of the MJO from the average of all eight phases of the MJO, the methodology utilized in Hall et al. (2001) is adopted here. This approach assumes that cyclone activity is uniformly distributed between all eight phases of the MJO, and consequently the z statistic calculated for significant differences is as follows:

$$z = \frac{p - p_0}{S_p}, \tag{1}$$

where p is the observed proportion of cyclogenesis activity to the number of total days within a particular MJO category, p_0 is the expected proportion of cyclogenesis activity to the total number of days within

TABLE 1. July–November-averaged values of 200-mb (1 mb = 1 hPa) zonal wind (U_{200}) ($m\,s^{-1}$), 850-mb zonal wind (U_{850}) ($m\,s^{-1}$), 200–850-mb zonal wind ($U_{200-850}$) shear ($m\,s^{-1}$), sea surface temperature (SST) (°C), sea level pressure (SLP) (hPa), outgoing longwave radiation (OLR) ($W\,m^2$), 300-hPa omega ($hPa\,day^{-1}$), 850-mb relative vorticity (RV_{850})($10^6\,s^{-1}$), and 700-mb relative humidity (RH_{700}) (%) in the North Atlantic MDR (10°–17.5°N, 75°–20°W). Values are calculated as deviations from the MJO phase 1–8 average when the WH MJO index is greater than one. Values that are significantly different at the 95% level from the phase 1–8 average are highlighted in boldfaced type.

Phase	U_{200}	U_{850}	$U_{200-850}$	SST	SLP	OLR	300-hPa omega	RV_{850}	RH_{700}
1	−2.30	0.21	−2.51	−0.03	−0.43	−1.56	−2.98	0.66	0.69
2	**−3.06**	0.55	**−3.62**	0.12	−0.32	−2.38	−4.01	0.64	1.47
3	−0.72	0.16	−0.87	0.02	0.21	0.61	1.95	−0.20	0.03
4	−0.35	0.18	−0.53	0.17	0.25	2.18	1.78	−0.05	0.12
5	0.27	−0.12	0.39	0.12	0.34	1.70	0.63	0.14	0.47
6	2.41	−0.37	2.78	−0.12	0.32	1.04	2.58	−0.22	−1.11
7	2.35	−0.61	**2.96**	**−0.27**	0.24	−0.27	0.80	−0.52	−1.71
8	1.40	−0.01	1.40	−0.02	**−0.61**	−1.32	−0.74	−0.44	0.04

a particular MJO category (e.g., 12.5%), and S_p is the estimator of the standard deviation of the fraction of cyclogenesis days, calculated as

$$S_p = \sqrt{p_0(1-p_0)/N}, \tag{2}$$

where N represents the number of days in a category. Assuming a Gaussian distribution, the critical z value needed for the 95% significance level is 1.96.

An additional significance test utilized here involves a Monte Carlo bootstrap resampling of the daily time series of TC activity (Efron 1979). The full time series of basinwide TC activity for all MJO phases is calculated, and then one-eigth of this time series is resampled to approximate the TC activity generated in a random subset of days that matches the number of days in a particular MJO phase. This procedure is done 10 000 times, the results are sorted, and the 5% and 95% confidence intervals are determined from the 500th and 9500th value obtained. Significance is only denoted if the particular TC metric investigated passes both the t test as well as the bootstrap resampling test. In general, the bootstrap resampling test seems to be a stricter requirement than the Hall et al. (2001) test.

As stated earlier, all calculations in the following sections are made for when the MJO index, as defined by Wheeler and Hendon (2004), has an amplitude greater than one.

3. MJO modulation in the North Atlantic Ocean

Analysis of the impacts of the MJO on TCs begins by examining large-scale environmental field modulation during the respective basin's TC season in the respective basin's MDR. For purposes of this study, TC season months are defined as those months when at least 95% of the basin's hurricanes (1-min sustained winds greater than or equal to 64 kt) form. The term "hurricane" is utilized for all basins, irrespective of the specific term typically utilized for a particular basin. Based on this classification scheme, the TC seasons are defined as follows: the North Atlantic Ocean from July to November, the northeast Pacific Ocean from June to October, the northwest Pacific Ocean from June to November, the north Indian Ocean from April to June and October to December, the south Indian Ocean from November to April, and the South Pacific Ocean from December to April. All TC statistics are calculated only for TCs forming in the months defined as the hurricane season in a particular basin.

Table 1 displays the modulation of large-scale environmental fields in the North Atlantic MDR (7.5°–22.5°N, 75°–20°W) based on MJO phase. As mentioned earlier, only days where the WH MJO index is greater than or equal to one are considered. Based upon previous research by the authors and others (e.g., Camargo et al. 2009), the following fields are examined for the North Atlantic as well as the remainder of the global TC basins: 200-mb zonal wind, 850-mb zonal wind, 200–850-mb zonal wind shear, sea surface temperature, sea level pressure, OLR, 300-hPa omega, 850-mb relative vorticity, and 700-mb relative humidity. Statistically significant differences at the 95% level utilizing a two-tailed Student's t test between the average of all eight phases and an individual phase are highlighted in boldfaced type. A total of 50 MJO events is conservatively estimated over the 34-yr period examined (approximately 1.5 coherent MJO events per basin hurricane season). The critical value needed for the 95% significance level is 2.01.

In general, deviations from the phase 1–8 average are not significant at the 95% level, except for phase 2, which exhibits deviations favorable for TC formation and phase 7, which exhibits deviations unfavorable for

TABLE 2. Named storms (NS), hurricanes (H), and major hurricanes (MH) forming in the Atlantic Ocean basin during each phase of the MJO when the WH index is greater than one. Positive differences from the phase 1–8 average that are significant at the 95% level are highlighted in boldfaced type, while negative differences from the phase 1–8 average that are significant at the 95% level are italicized. Also displayed is the percentage of total basin ACE generated by storms forming in each phase, the number of 24-h periods of RI of at least 30 kt, and the percentage chance of an individual TC undergoing RI of at least 30 kt at some point during its lifetime. A total of 136 Atlantic Ocean basin TCs underwent at least one 24-h RI period of 30 kt during the period from 1979 to 2011.

Phase	NS	H	MH	Basinwide ACE (%)	RI 24-h periods	RI chance (%)
1	7.4	4.7	2.0	19	13.9	50
2	**10.2**	**7.3**	**3.4**	**21**	**17.9**	49
3	8.2	3.1	2.1	11	4.5	*19*
4	8.6	6.3	2.0	17	11.3	38
5	5.9	3.5	1.5	9	8.1	48
6	5.8	3.3	*0.8*	*7*	*3.3*	*17*
7	*3.7*	*1.8*	1.1	*6*	4.8	40
8	6.2	2.9	1.1	10	7.3	35
Phase 1–8 avg	7.1	4.3	1.8	12	9.5	39

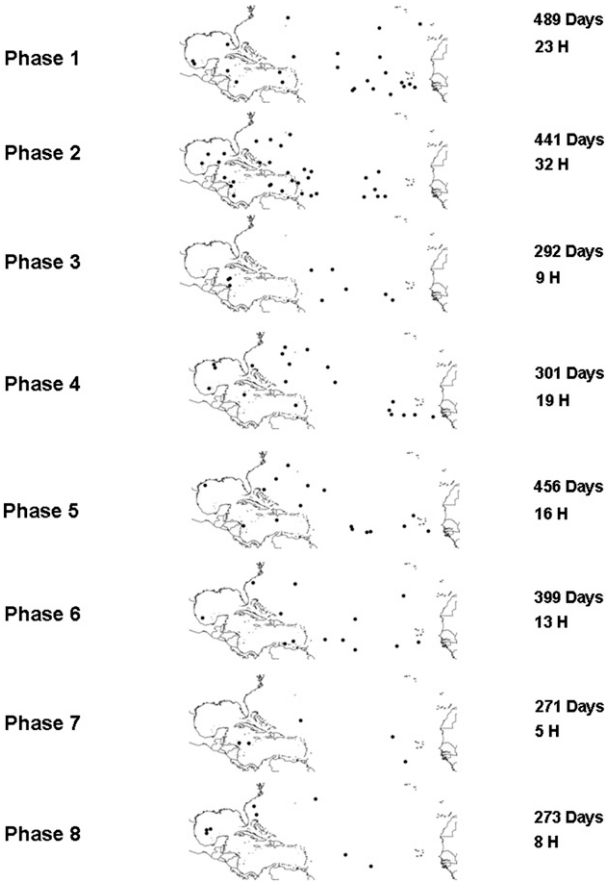

FIG. 2. Locations of named storm formation in the North Atlantic Ocean basin for each TC that reached hurricane (H) strength at some point during its lifetime. Also listed are the days that the MJO had an amplitude greater than one during the peak months of the TC season as defined in the text.

TC formation. In general, easterly deviations in 200–850-mb vertical shear are favorable for TC formation due to the climatological westerly shear that exists in most parts of the tropics. Differences between phases 2 and 7 are relatively strong for vertical wind shear (approximately $5\,m\,s^{-1}$), while differences are relatively small for OLR (about $2\,W\,m^{-2}$). Much stronger differences for OLR are observed in other TC basins (discussed in detail in the following sections).

Table 2 displays TC activity generated by storms forming in each phase of the MJO. All statistics are normalized by the number of days that the MJO spends in each phase with an amplitude greater than one during the period from July to November and then multiplied by 100, in keeping with the methodology of Klotzbach (2010). Individual phase differences that deviate positively from the average of all eight MJO phases that are significant at the 95% level are highlighted in boldfaced type, while negative deviations significant at the 95% level are italicized. Also displayed is the percentage of basinwide ACE generated by TCs forming in individual phases, the number of normalized 24-h RI periods of at least 30 kt and the percentage chance of a TC forming in each phase undergoing at least one RI episode of at least 30 kt.

TABLE 3. As in Table 1, but for the northeast Pacific Ocean MDR (10°–17.5°N, 140°–100°W).

Phase	U_{200}	U_{850}	$U_{200-850}$	SST	SLP	OLR	300-hPa omega	RV_{850}	RH_{700}
1	**−3.51**	**2.63**	**−6.13**	−0.07	−0.08	−1.71	**−5.40**	**1.89**	−1.47
2	−2.64	**1.95**	**−4.59**	−0.09	0.04	2.33	−0.13	0.80	−1.89
3	−0.57	0.13	−0.71	−0.08	0.10	**6.60**	**8.86**	−0.28	−2.29
4	1.54	**−1.52**	**3.06**	−0.01	0.12	**6.95**	**12.67**	**−1.44**	**−2.52**
5	1.86	**−2.26**	**4.12**	0.10	−0.06	1.43	4.96	**−1.96**	1.85
6	2.47	**−2.30**	**4.76**	0.07	0.06	−3.81	−2.65	**−1.55**	**2.79**
7	1.35	**−0.96**	2.31	0.08	0.03	**−7.24**	**−7.61**	0.65	**3.38**
8	−0.49	**2.33**	−2.82	0.00	−0.20	−4.55	**−10.70**	**1.90**	0.16

TABLE 4. As in Table 2, but for the northeast Pacific Ocean. A total of 195 northeast Pacific Ocean basin TCs underwent at least one 24-h RI period of 30+ kt during the period from 1979 to 2011.

Phase	NS	H	MH	Basinwide ACE (%)	RI 24-h periods	RI chance (%)
1	**12.4**	**7.3**	2.9	15	17.5	37
2	9.0	4.8	2.9	11	14.0	35
3	7.7	4.0	*0.8*	*7*	*7.3*	37
4	7.3	3.7	2.0	8	13.0	41
5	*4.9*	*2.2*	*1.3*	*5*	*5.1*	27
6	9.3	4.8	2.4	12	11.4	34
7	**13.0**	**7.3**	**4.5**	**20**	**22.4**	**50**
8	**14.0**	**8.6**	**4.5**	**21**	**23.3**	41
Phase 1–8 avg	9.6	5.2	2.6	12	13.9	38

Phases 1 and 2 tend to be associated with most TC formations, as well as most TCs undergoing RI and generating large levels of ACE. Phases 6 and 7 have statistically significant decreases from the all-phase average for ACE.

The chance of an individual storm undergoing RI is enhanced in phases 1, 2, and 5, while it is significantly reduced in phases 3 and 6. The significance of results for individual TCs undergoing RI should be taken with some caution, given that a fairly small sample size is being investigated here. In general, the modulations discussed above are to be expected given the changes in large-scale climate patterns discussed in detail in the previous paragraphs.

Figure 2 displays the named storm formation locations for all TCs that reached hurricane strength at some point during their lifetime. The number of days that the MJO was in a particular phase are also listed since the MJO preferentially spends more time in certain phases than in others. A significant cluster of TCs is evident in phases 1 and 2 in the MDR, in keeping with the results discussed in Klotzbach (2010). A paucity of TCs in the MDR is noted in phases 6 and 7. Large differences are also observed for the Gulf of Mexico and Caribbean, similar to what was discussed by Maloney and Hartmann (2000b). In phases 1 and 2, 17 TCs formed in the Gulf and Caribbean and reached hurricane strength, while only 5 TCs reaching hurricane strength formed in this region in phases 6 and 7.

4. MJO modulation in the northeast Pacific Ocean

Table 3 shows how large-scale fields are modified based on MJO phase for the northeast Pacific MDR (10°–17.5°N, 140°–100°W). In contrast to the North Atlantic, more MJO phases show significant differences from the phase 1–8 average for various large-scale fields.

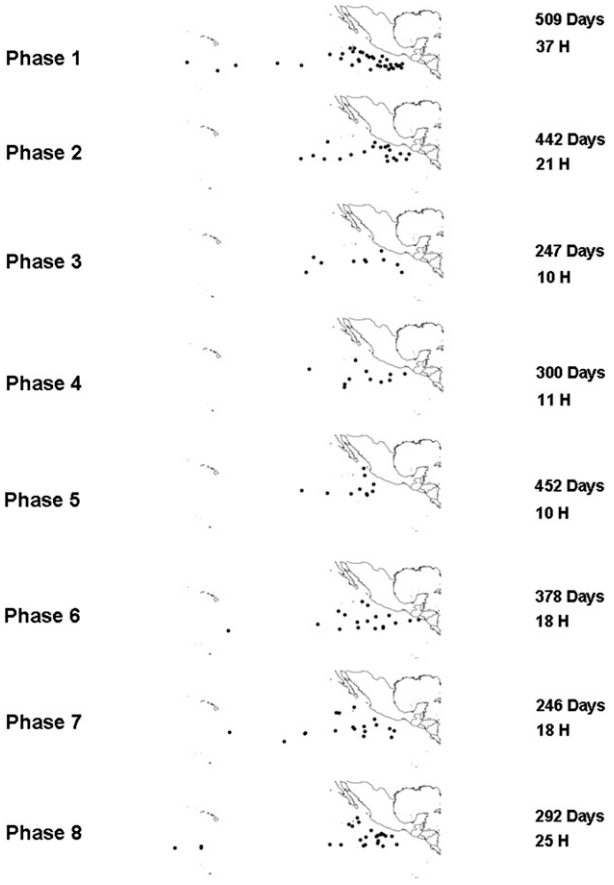

FIG. 3. As in Fig. 2, but for the northeast Pacific Ocean.

Also, magnitudes of differences between the lowest and the highest values for a particular large-scale field are also generally larger. For example, the largest difference in vertical wind shear in the North Atlantic is between phases 2 and 7 and is approximately $6.6\,\mathrm{m\,s^{-1}}$. The northeast Pacific has a somewhat larger difference, with the largest in magnitude being between phases 1 and 6 at $10.9\,\mathrm{m\,s^{-1}}$. Much larger differences are also noted for thermodynamic fields in the northeast Pacific compared with the North Atlantic. For example, the maximum difference magnitude between two MJO phases for OLR in the North Atlantic is $4.6\,\mathrm{W\,m^{-2}}$, compared with $14.2\,\mathrm{W\,m^{-2}}$ in the northeast Pacific. While magnitudes of modulation of thermodynamic fields are greater in the northeast Pacific than it is in the North Atlantic, it is still less than what will be seen for other TC basins, as the convective coupling of the MJO diminishes after reaching the cooler waters of the tropical eastern Pacific (Wheeler and Kiladis 1999).

Table 4 displays northeast Pacific TC activity generated by storms forming in each phase of the MJO along with RI statistics. Phases 1, 7, and 8 are generally associated with increased TC activity along with an increased

TABLE 5. As in Table 1, but for the northwest Pacific Ocean MDR (10°–20°N, 110°–170°E).

Phase	U_{200}	U_{850}	$U_{200-850}$	SST	SLP	OLR	300-hPa omega	RV_{850}	RH_{700}
1	−1.39	−0.11	−1.28	0.05	**0.90**	**8.52**	**11.60**	**−2.13**	−1.40
2	1.09	**−1.15**	2.25	0.09	**0.71**	**8.95**	**13.18**	**−2.13**	−2.42
3	**3.59**	**−1.91**	**5.50**	−0.06	0.45	**9.57**	**12.02**	**−2.01**	**−3.74**
4	2.54	**−1.15**	**3.69**	0.05	−0.25	−1.59	−0.39	−0.33	−0.41
5	0.48	0.05	0.44	0.09	**−0.83**	**−11.63**	**−15.93**	**1.92**	**3.49**
6	−1.16	**1.21**	−2.37	−0.02	**−0.93**	**−12.52**	**−16.68**	**2.48**	**3.28**
7	−2.72	**2.08**	**−4.80**	−0.15	**−0.69**	**−6.58**	**−9.48**	**2.57**	2.40
8	−2.44	**1.00**	**−3.44**	−0.06	**0.63**	5.27	5.69	−0.38	−1.21

number of 24-h RI periods. Phases 3–5 have reduced TC activity compared with the average of all eight MJO phases. Differences in the amount of ACE generated between MJO phases is quite large in the northeast Pacific, from 20% of all ACE in phases 7 and 21% of all ACE in phase 8 compared to only 5% in phase 5.

In general, the percentage chances of TCs undergoing RI at some point during their lifetime in the northeast Pacific does not change much from phase to phase of the MJO. The only statistically significant change from the phase 1–8 average of 38% is an increase to 50% in phase 7.

Figure 3 displays the named storm formation location for all TCs intensifying into hurricanes in the northeast Pacific. There is a large increase in TC formation in the northeast Pacific just off of the coast of Mexico in phases 8 and 1. Also, there tends to be enhanced TC formation in the north-central Pacific (west of 120°W) in phase 8, as noted in Klotzbach and Blake (2013). Activity is suppressed across the entire basin in phase 4 and especially in phase 5.

5. MJO modulation in the northwest Pacific Ocean

Table 5 displays large-scale field modifications based on MJO phase over the northwest Pacific MDR (10°–20°N, 110°–170°E). As was the case in the northeast Pacific, several MJO phases show significant differences from the phase 1–8 average for various large-scale fields. The magnitude of differences between the lowest and highest phases is much larger than for the Atlantic and somewhat larger than for the northeast Pacific. Vertical shear differences exceed $10\,m\,s^{-1}$ between phases 3 and 7, while the difference between phases 3 and 6 for OLR was over $20\,W\,m^{-2}$. Vertical motion differences approach 30 mb day^{-1} between phases 2 and 6, and relative vorticity differences near $5 \times 10^{-6}\,s^{-1}$ occur between phases 1 and 2 and phases 6 and 7. Given these anomalous differences one would expect a priori to see more TC activity in the northwest Pacific when the dynamic

TABLE 6. As in Table 2, but for the northwest Pacific Ocean. A total of 351 northwest Pacific Ocean basin TCs underwent at least one 24-h RI period of 30+ kt during the period from 1979 to 2011.

Phase	NS	H	MH	Basinwide ACE (%)	RI 24-h periods	RI chance (%)
1	9.5	7.3	3.8	12	19.2	49
2	*8.4*	6.3	3.2	9	16.8	**57**
3	*6.1*	*3.5*	*1.7*	*6*	*12.1*	43
4	9.0	*4.7*	2.9	*8*	15.3	35
5	**15.7**	9.3	4.6	14	23.5	36
6	**18.0**	**11.8**	4.8	**17**	27.6	34
7	**15.2**	**11.1**	**7.0**	**21**	**33.5**	50
8	9.5	6.6	3.7	12	22.6	**55**
Phase 1–8 avg	11.6	7.7	3.9	12	21.2	43

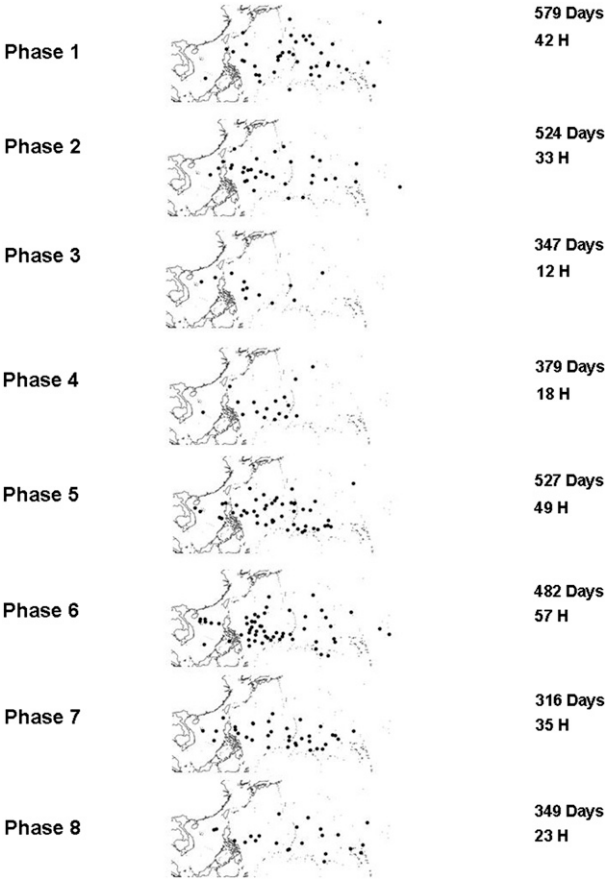

FIG. 4. As in Fig. 2, but for the northwest Pacific Ocean.

TABLE 7. As in Table 1, but for the north Indian Ocean MDR (7.5°–17.5°N, 65°–95°E).

Phase	U_{200}	U_{850}	$U_{200-850}$	SST	SLP	OLR	300-hPa omega	RV_{850}	RH_{700}
1	1.63	−0.52	2.15	0.18	0.09	−2.23	0.97	**−1.16**	**3.08**
2	1.13	**−1.45**	2.58	0.12	−0.50	**−10.48**	**−6.01**	−0.49	**4.71**
3	0.39	**−1.43**	1.82	−0.04	−0.39	**−10.88**	**−7.63**	0.49	2.34
4	**−3.63**	**0.76**	**−4.39**	0.06	**−0.97**	**−10.72**	**−13.07**	**1.94**	2.29
5	**−4.13**	**1.65**	**−5.78**	−0.14	**−0.53**	−2.16	−3.26	**1.97**	0.19
6	−1.61	**1.70**	**−3.31**	−0.11	0.30	**9.91**	**7.70**	0.34	**−3.58**
7	**3.50**	−0.20	**3.70**	−0.14	**1.23**	**17.70**	**13.26**	**−1.28**	**−6.97**
8	2.72	−0.52	**3.24**	0.07	**0.77**	**8.87**	**8.05**	**−1.81**	−2.07

and thermodynamic conditions are more favorable (e.g., phases 6 and 7) than when the conditions are less favorable (e.g., phases 2 and 3).

Table 6 displays normalized northwest Pacific TC activity generated by storms forming in each phase of the MJO along with RI statistics. In general, TC activity is most enhanced in phases 6 and 7, with significant reductions found in phases 3–4, similar to results found in Li and Zhou (2013). Nearly three times as many 24-h RI periods occur with TCs forming in phase 7 than forming in phase 3.

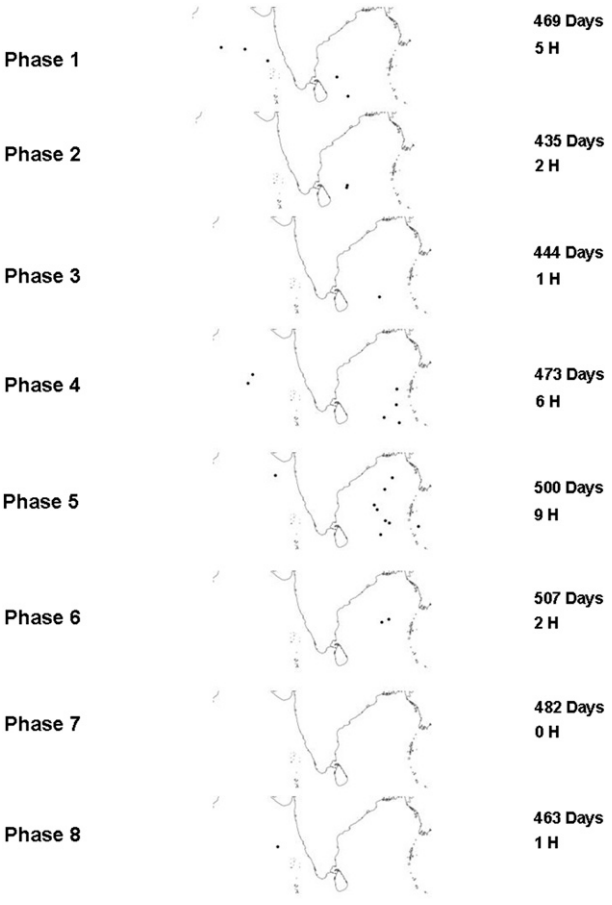

FIG. 5. As in Fig. 2, but for the north Indian Ocean.

While the number of 24-h periods is much greater for phases 6 and 7 than in phases 2 and 3, the chances of individual TCs undergoing RI at some point during their lifetime does not seem to be strongly related to favorable overall large-scale conditions. For example, TCs are significantly more likely to undergo RI in phase 2, despite the fact that overall TC formation in these phases is significantly less than the phase 1–8 average. Phase 8 also shows a significant increase in the likelihood of RI, even though TC activity in this phase is close to the phase 1–8 average.

Figure 4 displays the location where all TCs that reached H status at some point during their lifetime formed in the northwest Pacific. TC activity is raised throughout the basin in phases 6 and 7, but the most notable increase in activity relative to phases 2–4 is seen in the eastern part of the basin. This is to be expected, given the convective enhancement associated with the MJO is migrating from the western to the central Pacific during this time.

6. MJO modulation in the north Indian Ocean

MJO-driven large-scale field modulations in the north Indian Ocean MDR (7.5°–17.5°N, 65°–95°E) are displayed in Table 7. Significant differences are seen for

TABLE 8. As in Table 2, but for the north Indian Ocean. A total of 24 north Indian Ocean basin TCs underwent at least one 24-h RI period of 30+ kt during the period from 1979 to 2011.

Phase	NS	H	MH	Basinwide ACE (%)	RI 24-h periods	RI chance (%)
1	1.9	1.1	**0.6**	**23**	**4.3**	**44**
2	1.4	0.5	0.2	10	1.4	17
3	**4.5**	*0.2*	0.0	13	0.0	0
4	**3.6**	**1.3**	0.2	19	0.0	0
5	**4.2**	**1.8**	**0.8**	**25**	**4.2**	29
6	1.8	0.4	0.0	*3*	0.0	0
7	*0.4*	*0.0*	0.0	*2*	0.0	0
8	*0.4*	*0.2*	0.2	5	0.6	**50**
Phase 1–8 avg	2.3	0.7	0.1	12	1.3	14

TABLE 9. As in Table 1, but for the south Indian Ocean MDR (20°–10°S, 40°–130°E).

Phase	U_{200}	U_{850}	$U_{200-850}$	SST	SLP	OLR	300-hPa omega	RV_{850}	RH_{700}
1	**4.52**	**−1.04**	**5.56**	0.05	**0.78**	3.13	4.34	**2.43**	−0.96
2	2.36	**−1.20**	**3.56**	0.04	−0.27	−2.47	−2.55	**1.30**	2.06
3	−0.25	−0.41	0.16	0.01	**−0.83**	**−6.58**	**−6.60**	−0.11	**3.19**
4	−2.48	**0.70**	**−3.18**	−0.03	**−0.90**	**−6.00**	**−6.26**	**−1.61**	**3.20**
5	**−3.29**	**1.15**	**−4.44**	−0.04	−0.66	−1.88	−1.58	**−2.03**	0.77
6	−2.20	**0.68**	−2.88	−0.09	0.22	3.29	3.06	**−1.26**	**−2.31**
7	−0.92	0.53	−1.45	−0.03	**0.65**	**5.46**	4.83	−0.15	**−2.97**
8	2.26	−0.42	2.67	0.09	**1.01**	**5.06**	4.75	**1.43**	**−2.97**

most large-scale fields. OLR anomaly differences between various MJO phases are quite large, which is to be expected given that MJO events tend to initiate and have a strong amplitude in the Indian Ocean (e.g., Madden and Julian 1972). The difference in OLR between phases 2–4 and phase 7 approaches $30\,W\,m^{-2}$. Differences in other thermodynamic quantities are also quite large, with an approximately $25\,mb\,day^{-1}$ difference in vertical motion between phases 4 and 7, and a 12% difference in relative humidity between phases 2 and 7. Overall, the combination of dynamic and thermodynamic anomalies indicates that the most favorable conditions for TC formation and intensification are experienced over the Indian Ocean in phases 4 and 5, while phases 7 and 8 have the large-scale conditions most likely to suppress TC formation.

TC activity in the north Indian Ocean is enhanced in phases 1, 4, and 5 and is suppressed in phases 6–8. From examination of Fig. 5, it appears that the enhancement in phase 1 is primarily located in the Arabian Sea, while phases 4 and 5 are associated with enhanced activity in the Bay of Bengal. TC activity in both the Arabian Sea and the Bay of Bengal is a rare occurrence in phases 6–8. In general, TC formation in the north Indian Ocean occurs infrequently, and consequently the statistical significance of the results should be interpreted with caution. RI is generally a rare event in the north Indian Ocean, so the number of 24-h periods and the percentage chance of RI have less relevance in this basin than in the other basins examined in this manuscript (Table 8). It is impossible to test for statistical significance of the low extreme (e.g., 5% level) for major hurricanes, 24-h RI periods and chance of RI, given that each of these have over 500 zero values when the Monte Carlo test is run.

The NS formation point for all TCs that reached H status in the north Indian Ocean are displayed in Fig. 5.

TABLE 10. As in Table 2, but for the south Indian Ocean. A total of 174 south Indian Ocean basin TCs underwent at least one 24-h RI period of 30+ kt during the period from 1979 to 2011.

Phase	NS	H	MH	Basinwide ACE (%)	RI 24-h periods	RI chance (%)
1	*4.9*	3.3	*1.3*	*8*	6.4	42
2	7.5	5.1	**3.6**	16	**15.6**	**51**
3	**10.6**	**5.8**	3.2	**18**	14.6	32
4	**12.0**	**5.9**	**3.9**	**18**	**15.7**	34
5	**11.9**	4.5	3.4	**17**	14.2	26
6	8.0	5.0	3.0	13	9.7	38
7	*5.0*	*2.3*	*0.7*	*6*	*3.2*	*18*
8	*3.8*	*2.2*	*0.9*	*5*	*4.4*	35
Phase 1–8 avg	8.0	4.3	2.5	12	10.5	34

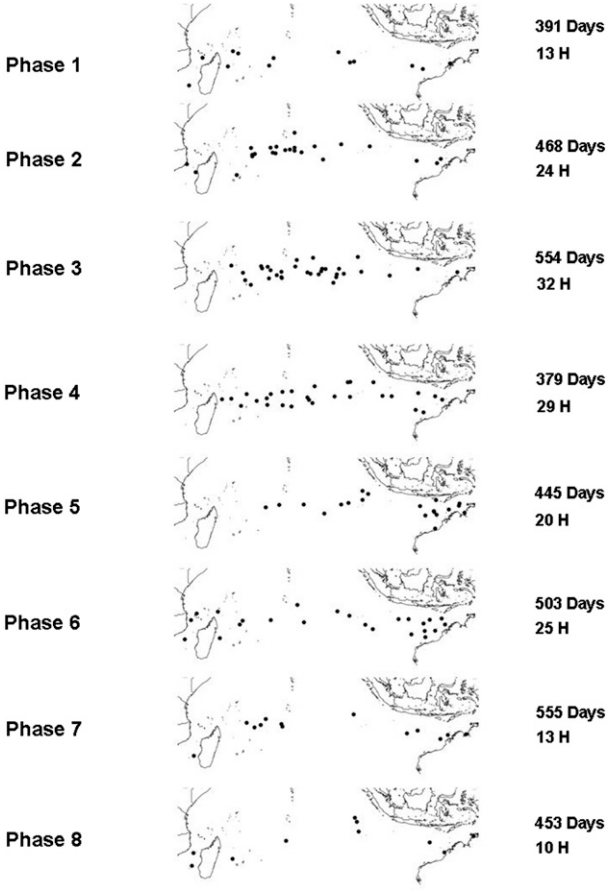

FIG. 6. As in Fig. 2, but for the south Indian Ocean.

TABLE 11. As in Table 1, but for the South Pacific Ocean MDR (20°–10°S, 135°E–150°W).

Phase	U_{200}	U_{850}	$U_{200-850}$	SST	SLP	OLR	300-hPa omega	RV_{850}	RH_{700}
1	−0.58	0.18	−0.76	−0.07	**1.23**	**8.32**	**6.17**	−0.32	**−4.34**
2	−0.46	**−1.33**	0.88	0.01	**1.09**	**6.83**	**7.81**	**1.19**	−2.30
3	1.44	**−1.97**	**3.41**	0.01	0.39	**4.74**	**7.65**	**1.95**	−1.91
4	1.94	**−1.77**	**3.71**	0.00	−0.12	−0.30	2.00	**1.72**	0.41
5	0.74	**−0.82**	1.57	0.07	**−0.56**	−3.11	−2.02	**1.14**	**2.70**
6	0.20	**1.05**	−0.85	0.06	**−1.15**	**−9.82**	**−9.36**	**−1.06**	**3.50**
7	−1.63	**2.53**	**−4.16**	−0.04	**−0.97**	**−8.63**	**−11.80**	**−2.63**	**2.98**
8	−1.65	**2.13**	**−3.79**	−0.04	0.10	1.98	−0.44	**−1.99**	−1.04

Three H formed in the Arabian Sea in phase 1, while only four H formed in the Arabian Sea in the remaining seven MJO phases. Likewise, in the Bay of Bengal, 12 hurricanes formed in phases 4 and 5, while only 7 hurricanes formed in the remaining six phases of the MJO, in keeping with the results of Kikuchi and Wang (2010). While the sample size for north Indian Ocean TCs is smaller than that of any of the other ocean basins examined here, there appears to be a very strong MJO–TC relationships in this basin.

7. MJO modulation in the south Indian Ocean

The focus of this manuscript now shifts to the Southern Hemisphere. Table 9 displays how large-scale fields are modulated by the MJO in the south Indian Ocean MDR (20°–10°S, 40°–130°E). Approximately $10\,m\,s^{-1}$ difference in vertical shear is noted between phases 1 and 5. Large differences are also noted for relative vorticity, with a $4.5 \times 10^{-6}\,s^{-1}$ increase in cyclonic relative vorticity (negative in the Southern Hemisphere) noted for phase 5 compared to phase 1, similar to results found by Bessafi and Wheeler (2006). Generally, the most favorable large-scale conditions in the south Indian Ocean are typically associated with phases 3–5, while the least conducive conditions are associated with phases 7, 8, and 1.

TABLE 12. As in Table 2, but for the South Pacific Ocean. A total of 106 South Pacific Ocean basin TCs underwent at least one 24-h RI period of 30+ kt during the period from 1979 to 2011.

Phase	NS	H	MH	Basinwide ACE (%)	RI 24-h periods	RI chance (%)
1	5.0	2.8	1.6	11	6.9	44
2	*3.9*	*1.6*	1.0	6	5.2	27
3	*3.5*	*2.0*	1.1	12	3.5	31
4	4.4	2.2	1.0	*6*	4.4	22
5	*4.1*	*1.9*	*0.5*	*7*	5.9	40
6	**8.5**	4.5	1.8	16	11.3	35
7	**10.3**	**5.2**	**3.1**	**22**	8.9	28
8	7.3	**4.8**	2.5	20	**13.4**	45
Phase 1–8 avg	6.0	2.9	1.6	12	7.4	34

As would be expected given the large-scale modulations discussed in the previous paragraph, significant differences in TC activity are observed in the south Indian Ocean when evaluated by the ACE metric. TC activity is enhanced in phases 3–5, with suppression noted in phases 7, 8, and 1. There are approximately three times as many 24-h RI periods in phases 2–5 than there are in phases 7, 8, and 1 (Table 10).

Over half of all TCs forming in the south Indian Ocean in phase 2 undergo RI at some point during their lifetime, compared with only 18% in phase 7. The increased chance of RI in phase 2 may be due to the

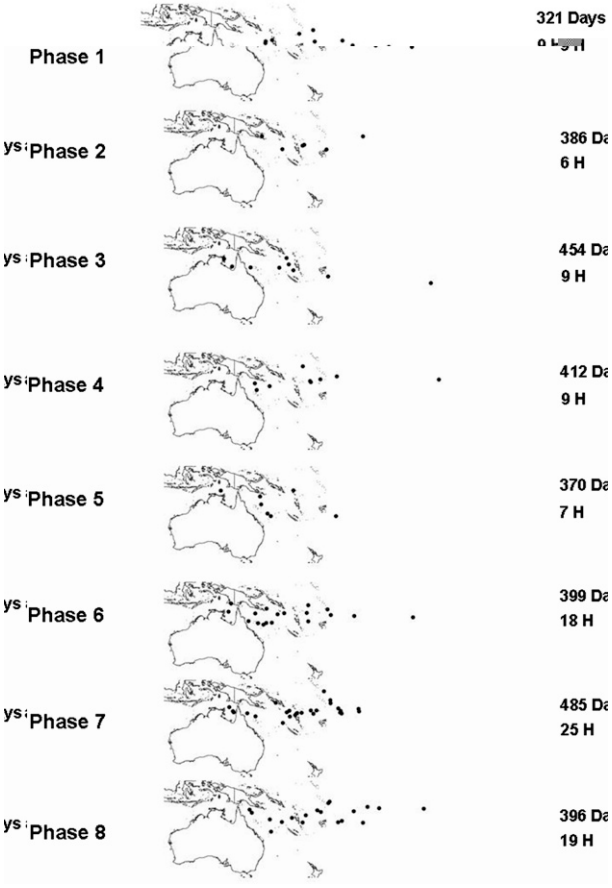

FIG. 7. As in Fig. 2, but for the South Pacific Ocean.

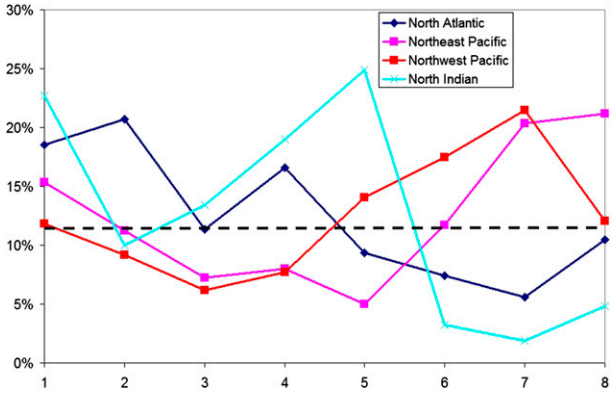

FIG. 8. Normalized per Northern Hemisphere TC basin ACE by MJO phase. The cyan line represents the north Indian Ocean basin, the dark blue line represents the North Atlantic Ocean basin, the purple line represents the northeast Pacific basin, and the dark red line represents the northwest Pacific basin. The dashed solid line represents the average activity expected per phase if the MJO did not modify activity (e.g., 12.5%).

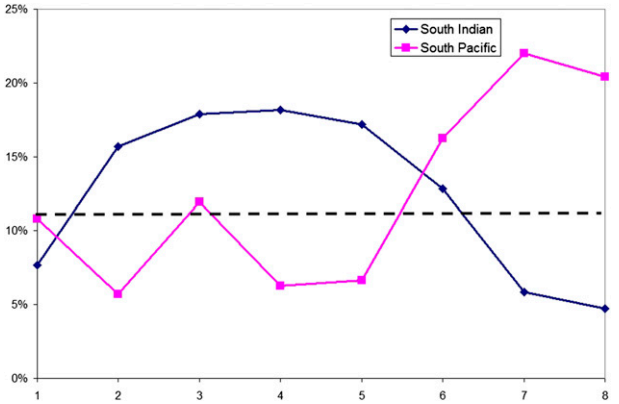

FIG. 9. As in Fig. 8, but for the Southern Hemisphere. The dark blue line represents the south Indian Ocean, while the purple line represents the South Pacific Ocean.

location of where TCs form in this particular phase, as they tend to form away from landmasses and therefore avoid inhibiting factors associated with land. Phase 7 tends to be associated with the suppressed convective phase of the MJO over the south Indian Ocean, and consequently, TCs that form in this particular phase tend to face an unfavorable environment for intensification.

Figure 6 displays the locations of NS formation for all TCs reaching H strength in the south Indian Ocean. Several interesting observations are noted from this figure. There is generally an eastward shift in the TC genesis region, which tends to coincide with where the MJO is enhancing convection. For example, while phases 3–5 tend to be the most active phases overall for the south Indian Ocean basin, no TCs have formed and reached H strength in any of these three phases in the Mozambique Channel. TC activity near the Australian coast (east of 110°E) occurs at a much higher rate in phases 5 and 6 (19 H formations) than in phases 8 and 1 (5 H formations).

8. MJO modulation in the South Pacific Ocean

Table 11 displays how large-scale fields are modulated by the MJO during the hurricane season in the South Pacific Ocean MDR (20°–10°S, 135°E–150°W). The most TC-favorable conditions from a thermodynamic perspective appear to be phases 6 and 7, while the most TC-favorable conditions from a dynamic perspective lag slightly in phases 7 and 8. A similar lag is observed for TC-suppressed environments. Phases 1 and 2 tend to be associated with the least favorable thermodynamic conditions, while phases 3 and 4 are associated with the least favorable dynamic conditions.

Statistically significant increases in South Pacific TC activity are demonstrated for H in phases 7 and 8, coinciding with the most favorable dynamic conditions across the basin (Table 12). There tends to generally be a broad reduction in TC activity in phases 2–5. There are more than three times as many 24-h RI periods in phase 8 compared with phases 3 and 4.

Broadly speaking, there appears to be an increase in an individual TC's chance of undergoing RI relative to climatology in phases 8 and 1, with a reduced chance for an individual TC of undergoing RI in phases 2–4.

The NS formation location for all TCs forming in the South Pacific is displayed in Fig. 7. In general, the most favored areas for TC formation tend to shift eastward as the MJO progresses eastward. Considerable differences are observed for H forming in the eastern part of the South Pacific (east of 175°E) between phases 4 and 5 versus phases 7 and 8. A total of 22 H formed east of 175°W in phases 7 and 8 compared with only three H in phases 4 and 5. This type of relationship is to be expected, given that the convectively favorable portion of the MJO is emerging in the Western Hemisphere during these two phases.

9. Summary and future work

This manuscript documents how tropical cyclones in each of the global TC basins are modulated by the MJO. Generally speaking, TC activity is enhanced during and immediately following the active convective phase of the MJO, with TC activity suppressed during and immediately following the convectively suppressed phase. Figure 8 displays the percentage of the normalized accumulated cyclone energy generated by TCs forming in each phase of the MJO for the four TC basins examined

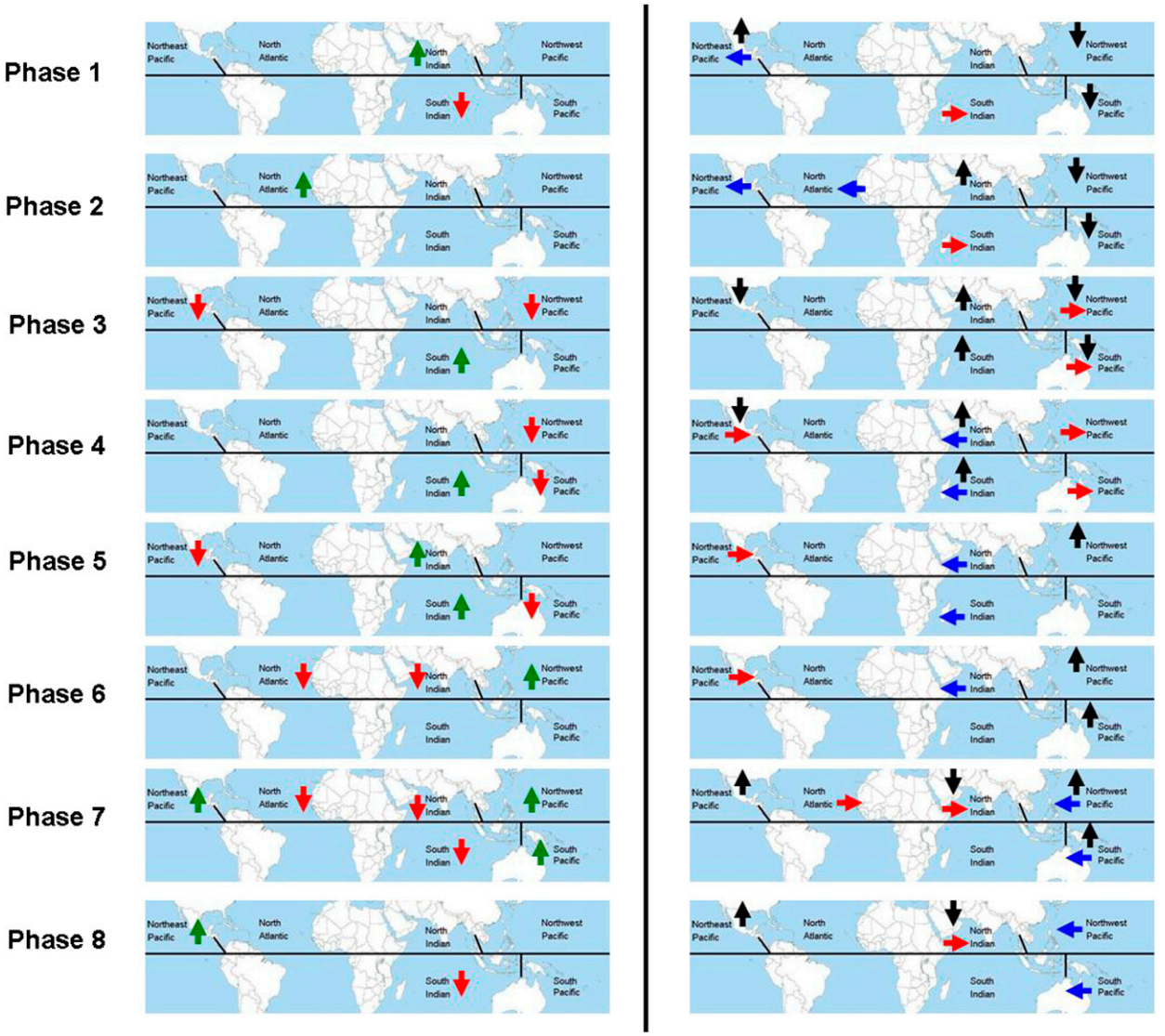

FIG. 10. (left) Statistically significant increases (green upward-pointing arrows) and statistically significant decreases (red downward-pointing arrows) in ACE from the phase 1–8 average by tropical cyclone basin. (right) Statistically significant differences in 200–850-mb vertical shear (westerly shear anomalies in red, easterly shear anomalies in blue) and 300-hPa omega (up arrows represent upward motion, down arrows represent downward motion) from the phase 1–8 average.

in the Northern Hemisphere. On a normalized basis, North Atlantic ACE peaks in phases 1–2 of the MJO, with the primary peak in north Indian Ocean ACE occurring in phases 3–5 (with a secondary peak in phase 1), followed by the northwest Pacific in phases 6 and 7 and the northeast Pacific in phase 8. In the Southern Hemisphere, south Indian Ocean TC activity is generally enhanced in phases 2–5, with South Pacific Ocean TC activity enhanced in phases 6–8 and 1 (Fig. 9). These observations tend to validate the statements in Gray (1979) that TCs typically cluster in time for various parts of the globe.

The primary reason why TC modulation is as observed is because of changes in large-scale fields, both dynamic and thermodynamic. While the Atlantic basin tends to have the least phase-by-phase modulation by the MJO, it still exhibits large differences in TC activity. The north Indian Ocean and northwest Pacific Ocean have the largest changes in the thermodynamic fields examined here, such as OLR and vertical motion. In general, the most active phases for TC activity coincide with the most favorable combination of dynamic and thermodynamic conditions.

Figure 10 provides a summary of the findings of this paper, both in terms of large-scale field modulations as

well as TC activity modulations. In general, TC activity is enhanced in a particular basin when both vertical shear is reduced and vertical motion is enhanced. The figure also clearly shows eastward propagation of TC-favored areas as the MJO propagates around the globe.

The focus of this study was over the time period from 1979 to 2012. Recently, an extended MJO dataset since 1905 using surface pressure has been developed by Oliver and Thompson (2012), and this dataset will be examined for potential evaluation of longer-term MJO signals with global TC data, recognizing that uncertainties in large-scale fields, MJO location, and intensity and TC activity all increase as one goes further back in time. A longer time series of MJO data will allow for the potential to investigate relationships between the MJO and other seasonal to multidecadal climate anomalies such as the Atlantic multidecadal oscillation (Goldenberg et al. 2001) and the El Niño–Southern Oscillation (Rasmusson and Carpenter 1982). These relationships will be investigated in future work.

Acknowledgments. Valuable discussions on the MJO and its relationships with global TCs were held with William Gray, Eric Blake, and Matthew Wheeler.

REFERENCES

Aiyyer, A., and J. Molinari, 2008: MJO and tropical cyclogenesis in the Gulf of Mexico and eastern Pacific: Case study and idealized numerical modeling. *J. Atmos. Sci.,* **65,** 2691–2704.

Barrett, B. S., and L. M. Leslie, 2009: Links between tropical cyclone activity and Madden–Julian oscillation phase in the North Atlantic and northeast Pacific basins. *Mon. Wea. Rev.,* **137,** 727–744.

Bell, G. D., and Coauthors, 2000: Climate assessment for 1999. *Bull. Amer. Meteor. Soc.,* **81,** S1–S50.

Bessafi, M., and M. C. Wheeler, 2006: Modulation of south Indian Ocean tropical cyclones by the Madden–Julian oscillation and convectively coupled equatorial waves. *Mon. Wea. Rev.,* **134,** 638–656.

Camargo, S. J., M. C. Wheeler, and A. H. Sobel, 2009: Diagnosis of the MJO modulation of tropical cyclogenesis using an empirical index. *J. Atmos. Sci.,* **66,** 3061–3074.

Chand, S. S., and K. J. E. Walsh, 2010: The influence of the Madden–Julian oscillation on tropical cyclone activity in the Fiji region. *J. Climate,* **23,** 868–886.

Chu, J.-H., C. R. Sampson, A. S. Levin, and E. Fukada, 2002: The Joint Typhoon Warning Center tropical cyclone best-tracks, 1945–2000. Naval Research Laboratory Rep. NRL/MR/7540-02-16, 22 pp.

Davis, M. A. S., G. M. Brown, and P. Leftwich, 1984: A tropical cyclone data tape for the eastern and central North Pacific basins, 1949–1983: Contents, limitations, and uses. NOAA Tech. Memo. NWS/NHC-25, Miami, FL, 17 pp.

Dee, D. P., and Coauthors, 2011: The ERA-Interim reanalysis: Configuration and performance of the data assimilation system. *Quart. J. Roy. Meteor. Soc.,* **137,** 553–597, doi:10.1002/qj.828.

Dvorak, V. F., 1982: Tropical cyclone intensity analysis and forecasting from satellite visible or enhanced infrared imagery. NOAA/National Environmental Satellite Service, Applications Laboratory Training Notes, 42 pp.

Efron, B., 1979: Bootstrap methods: Another look at the jackknife. *Ann. Stat.,* **7,** 1–26.

Goldenberg, S. B., C. W. Landsea, A. M. Mestas-Nuñez, and W. M. Gray, 2001: The recent increase in Atlantic hurricane activity: Causes and implications. *Science,* **293,** 474–479.

Gray, W. M., 1979: Hurricanes: Their formation, structure and likely role in the tropical circulation. *Meteorology over Tropical Oceans,* D. B. Shaw, Ed., Royal Meteorological Society, 155–218.

Hall, J. D., A. J. Matthews, and D. J. Karoly, 2001: The modulation of tropical cyclone activity in the Australian region by the Madden–Julian oscillation. *Mon. Wea. Rev.,* **129,** 2970–2982.

Ho, C.-H., J.-H. Kim, J.-H. Jyong, H.-S. Kim, and D. Chen, 2006: Variation of tropical cyclone activity in the south Indian Ocean: El Niño–Southern Oscillation and Madden–Julian oscillation effects. *J. Geophys. Res.,* **111,** D22101, doi:10.1029/2006JD007289.

Jarvinen, B. R., C. J. Neumann, and M. A. S. Davis, 1984: A tropical cyclone data tape for the North Atlantic basin, 1886-1983: Contents, limitations, and uses. NOAA Tech. Memo. NWS/NHC-22, Miami, FL, 21 pp.

Kaplan, J., and M. DeMaria, 2003: Large-scale characteristics of rapidly intensifying tropical cyclones in the North Atlantic basin. *Wea. Forecasting,* **18,** 1093–1108.

Kikuchi, K., and B. Wang, 2010: Formation of tropical cyclones in the northern Indian Ocean associated with two types of tropical intraseasonal oscillation modes. *J. Meteor. Soc. Japan,* **88,** 475–496.

Kim, J.-H., C.-H. Ho, H.-S. Kim, C.-H. Sui, and S. K. Park, 2008: Systematic variation of summertime tropical cyclone activity in the western North Pacific in relation to the Madden–Julian oscillation. *J. Climate,* **21,** 1171–1191.

Klotzbach, P. J., 2010: On the Madden–Julian oscillation–Atlantic hurricane relationship. *J. Climate,* **23,** 282–293.

——, 2012: El Niño–Southern Oscillation, the Madden–Julian oscillation and Atlantic basin tropical cyclone rapid intensification. *J. Geophys. Res.,* **117,** D14104, doi:10.1029/2012JD017714.

——, and E. S. Blake, 2013: North-central Pacific tropical cyclones: Impacts of El Niño–Southern Oscillation and the Madden–Julian oscillation. *J. Climate,* **26,** 7720–7733.

Krishnamohan, K. S., K. Mohanakumar, and P. V. Joseph, 2012: The influence of Madden–Julian oscillation in the genesis of north Indian Ocean tropical cyclones. *Theor. Appl. Climatol.,* **109,** 271–282.

Leroy, A., and M. C. Wheeler, 2008: Statistical prediction of weekly tropical cyclone activity in the Southern Hemisphere. *Mon. Wea. Rev.,* **136,** 3637–3654.

Li, R. C. Y., and W. Zhou, 2013: Modulation of western North Pacific tropical cyclone activity by the ISO. Part I: Genesis and intensity. *J. Climate,* **26,** 2904–2918.

Liebmann, B., and C. A. Smith, 1996: Description of a complete (interpolated) outgoing longwave radiation dataset. *Bull. Amer. Meteor. Soc.,* **77,** 1275–1277.

——, H. H. Hendon, and J. D. Glick, 1994: The relationship between tropical cyclones of the western Pacific and Indian Ocean and the Madden–Julian oscillation. *J. Meteor. Soc. Japan,* **72,** 401–412.

Madden, R. A., and P. R. Julian, 1972: Description of global-scale circulation cells in the tropics with a 40–50 day period. *J. Atmos. Sci.,* **29,** 1109–1123.

——, and ——, 1994: Observations of the 40–50-day oscillation—A review. *Mon. Wea. Rev.,* **122,** 814–837.

Maloney, E. D., and D. L. Hartmann, 2000a: Modulation of eastern North Pacific hurricanes by the Madden–Julian oscillation. *J. Climate,* **13,** 1451–1460.

——, and ——, 2000b: Modulation of hurricane activity in the Gulf of Mexico by the Madden–Julian oscillation. *Science,* **287,** 2002–2004.

Oliver, E. C. J., and K. R. Thompson, 2012: A reconstruction of Madden–Julian oscillation variability from 1905 to 2008. *J. Climate,* **25,** 1996–2019.

Ramsay, H. A., S. J. Camargo, and D. Kim, 2012: Cluster analysis of tropical cyclone tracks in the Southern Hemisphere. *Climate Dyn.,* **39,** 897–917, doi:10.1007/s00382-011-1225-8.

Rasmusson, E. M., and T. H. Carpenter, 1982: Variations in tropical sea surface temperature and surface wind fields associated with the Southern Oscillation/El Niño. *Mon. Wea. Rev.,* **110,** 354–384.

Roundy, P. E., C. J. Schreck III, and M. A. Janiga, 2009: Contributions of convectively coupled equatorial Rossby waves and Kelvin waves to the real-time multivariate MJO indices. *Mon. Wea. Rev.,* **137,** 469–478.

Ventrice, M. J., C. D. Thorncroft, and P. E. Roundy, 2011: The Madden–Julian oscillation's influence on African easterly waves and downstream tropical cyclogenesis. *Mon. Wea. Rev.,* **139,** 2704–2722.

Wheeler, M. C., and G. N. Kiladis, 1999: Convectively coupled equatorial waves: Analysis of clouds in the wavenumber–frequency domain. *J. Atmos. Sci.,* **56,** 374–399.

——, and H. H. Hendon, 2004: An all-season real-time multivariate MJO index: Development of an index for monitoring and prediction. *Mon. Wea. Rev.,* **132,** 1917–1932.